Polyhedron 175 (2020) 114180

Contents lists available at ScienceDirect

Polyhedron

journal homepage: www.elsevier.com/locate/poly

Hybrid halobismuthates as prospective light-harvesting materials: Synthesis, crystal, optical properties and electronic structure

George C. Anyfantis [a,*], Anna Ioannou [a], Hamdi Barkaoui [b], Younes Abid [b], Vassilis Psycharis [c], Catherine P. Raptopoulou [c], George A. Mousdis [a,*]

[a] National Hellenic Research Foundation, Theoretical and Physical Chemistry Institute, Vass. Constantinou Ave., 48, 116-35 Athens, Greece
[b] University of Sfax, Laboratoire de Physique Appliqué, Faculté des Sciences de Sfax, BP 1171 Sfax, Tunisia
[c] NCSR, Demokritos, Institute of Nanoscience and Nanotechnology, 15310 Aghia Paraskevi, Attiki, Greece

ARTICLE INFO

Article history:
Received 8 July 2019
Accepted 13 October 2019
Available online 21 October 2019

Keywords:
Low-dimensional bismuth compounds
Organic–inorganic hybrid composites
Optical properties
Crystal structure
Theoretical calculations

ABSTRACT

In the present paper, the synthesis, X-ray structural characterization, optical properties and electronic structures of three novel organic–inorganic hybrid compounds of the general formula $[CH_3SC(NH_2)_2]_xBiA_{x+3}$, (A = I, Br, Cl, and x = 1 or 2) are reported. All of them show intense narrow excitonic peaks at the absorption spectra and narrow photoluminescence bands. In the case of (x = 1 and A = I) its structure consists of edge sharing BiI_6 octahedral forming zigzag chains and in the case of (x = 2 and A = Br, Cl) their structure consists of corner sharing BiX_6 octahedral also forming zigzag chains. The amine group is located in the free cavities between the chains. Their structural, optical and vibronic properties were studied. Band structure calculations were made in order to compare the results with the experimental findings and gain an insight of the properties of these new compounds.

1. Introduction

One of the most successful strategies to obtain novel functional materials is to combine the specific properties of the inorganic frameworks, such as electronic properties, and the intriguing features of the organic ligands, such as flexibility and the ability to form weak interactions. An emerging class of these materials is the organic–inorganic hybrid halometalates. These materials are low cost and solution processable semiconducting materials. They show excellent optoelectronic properties such as high and balanced carrier mobility [1,2], long carrier diffusion length [3], large light absorption coefficient in the UV–vis range, [4,5] nonlinear optical effects [6] and efficient luminescence [7,8]. They combine the favourable properties of the inorganic semiconductor, namely its excellent charge carrier mobility, with the flexibility and low-temperature fabrication process ability, of the organic material [9]. They have the general formula $A_xM_yX_z$ where A = organic amine or diamine, M = Pb, Sn, Bi, Sb or other metal and X = I, Br, Cl. These materials consist of distorted anionic $[MX_6]^n$ octahedral [10], which share corners, edges, or faces to form discrete or extended three, two or one dimensional inorganic networks. The organic moiety is placed between those networks controlling the structure through its size and hydrogen and/or van der Waals bonds. The inorganic networks act as semiconductors (physical quantum wells, wires or dots in the case of 2, 1, or 0 dimensional inorganic networks, respectively) and the amines act as physical and electronic barrier, contributing to original electrical and optical behaviour [11]. By choosing the appropriate components, tailor-made materials with desirable structures and properties can be prepared. For instance, a wide range of organic amines with different sizes and functionalities, including alkyl and/or aromatic amines can be used, to differentiate their properties.

Lately the interest in hybrid halometalates and especially, the halogenplumbates with a three-dimensional (3D) perovskite type crystal structure is expanded. They have emerged as one of the most promising materials for next-generation photovoltaic solar cells (PSCs). These materials have been used in various architectures of solid-state PSCs, including the meso-superstructured scaffold [12], the planar structure [13] and even metal oxide-free geometries [14], increasing the energy transformation efficiency from 3.8% [15] to the appreciable level of more than 20% [16,17].

Moreover, due to their unique physical properties these materials have been studied as elements of nonlinear optical devices [18,19], light emitting diodes (LEDs) [20,21], photoconductors [22], optical microcavities [23] and as channels of thin-film field-effect transistors [24].

* Corresponding authors.
E-mail addresses: gc.anyfantis@gmail.com (G.C. Anyfantis), gmousdis@eie.gr (G.A. Mousdis).

https://doi.org/10.1016/j.poly.2019.114180
0277-5387/

There are still various problems concerning mainly the most studied lead based hybrid halometalates that impede their commercial use. These barriers are associated with the stability and mostly with the toxicity of the containing lead, which is readily bioavailable due to the instant solubility in water. For this reason, similar materials based on other metals were proposed for replacing the hybrid haloplumbates as candidates for the different applications. A promising candidate is the halobismuthates of the type A_nBiX_{n+3} [25].

Bismuth is the only one from the 6p-block elements with an outer lone pair of $6s^2$ electron same as lead. In advance, bismuth has low toxicity. This is probably because of the great insolubility of its salts that prevents their absorption and their physical qualities that are demulcent and protective of mucous membranes and skin.

The simple iodide BiI_3 is a semiconductor with a band gap ~1.8 eV and has been investigated as candidate for PSCs absorber [26]. Although there are many studies investigating the rich structural variety of the hybrid organic–inorganic bismuth halides, there are only few studies concerning the study of their optoelectronic properties [27]. Recently, it has been demonstrated that some halobismuthates can be used as the active layer in photovoltaic devices [28–30]. Although their yield is still very low, they present very good stability [31]. The majority of halobismuthates that have been tested for photovoltaic applications have a 0D structure with the general formula $A_3Bi_2I_9$ (a = CH_3NH_3 or Cs) [28,32], also some 1D compounds with a formula $ABiI_4$, have been tested [33]. We expect that if we increase the dimensionality of the compounds, we will increase the yield by decreasing the band gap and improving the electronic properties.

In the present paper the synthesis, structure and optical properties of three hybrid halobismuthates with the $CH_3SC(NH_2)_2^+$ cation are described. The results are compared with those observed from similar Low-Dimensional (LD) compounds based on inorganic units.

2. Experimental section

2.1. Starting materials

The following starting materials were used without further purification. Bismuth subcarbonate (Aldrich Chemical Company, CAS Number: 5892-10-4), hydroiodic acid 57% (Merck 341), hydrobromic acid 47% (Merck 304), hydrochloric acid 25% (Merck 312). The preparation of amine salts $CH_3SC(NH_2)_2I$, $CH_3SC(NH_2)_2Br$ and $CH_3SC(NH_2)_2Cl$ were described in previous papers [10,34].

2.2. Synthesis of $[CH_3SC(NH_2)_2]BiI_4$ (1)

0.153 g of $(BiO)_2CO_3$ (0.3 mmol) and 0.262 g of $CH_3SC(NH_2)_2I$ (1.2 mmol) were dissolved in 3 ml of HI and refluxed for 1 hour. The solution was concentrated to a volume of 1 ml and cooled to 0 °C for 12 h to give black-red crystals. The crystals were filtrated and left under vacuum for 8 hours to dry and remove any traces of HI. It gave 0.291 g (0.36 mmol) (Yield 60.0%, mp: 178 °C). ICP-MS analysis for $C_2H_7BiI_4N_2S$ Calc. %Bi: 25.87%, Experimental %Bi: 25.90%.

2.3. Synthesis of $[CH_3SC(NH_2)_2]_2BiBr_5$ (2)

0.102 g of $(BiO)_2CO_3$ (0.2 mmol) and 0.137 g of $CH_3SC(NH_2)_2Br$ (0.8 mmol) were dissolved in 5 ml of HBr and refluxed for 2 hours. The solution was concentrated to a volume of 1 ml and cooled to 0 °C for 12 h to give yellow crystals. The crystals were filtrated and left under vacuum for 8 h to dry and remove any traces of HBr. (196 mg 0.25 mmol, Yield 62%, mp: 184 °C). ICP-MS analysis for $C_4H_{14}BiBr_5N_4S_2$ Calc. %Bi: 26.43%, Experimental %Bi: 26.82%.

2.4. Synthesis of $[CH_3SC(NH_2)_2]_2BiCl_5$ (3)

0.255 g of $(BiO)_2CO_3$ (0.5 mmol) and 0.253 g of $CH_3SC(NH_2)_2Cl$ (2 mmol) were dissolved in 5 ml of HCl and refluxed for 2 hours. The solution was left in open air to concentrate and white crystals were formed. The crystals were filtrated and left under vacuum for 8 hours to dry and remove any traces of HCl. (0.313 g 0.55mmole, Yield 55%, mp: 155 °C). ICP-MS analysis for $C_4H_{14}BiBr_5N_4S_2$ Calc. %Bi: 36.76%, Experimental %Bi: 36.41%.

2.5. Melting points

The melting points were determined using a Buchi "Dr. Tottoli" melting point apparatus, in open-end capillaries, at a ramp rate of 120 (a.u.). The melting points are not corrected.

2.6. Chemical analysis

The chemical analysis was done by Inductively Coupled Plasma Mass Spectrometry using the Perkin Elmer SCIEX, Canada 9000 Series ICP-MS instrument. Operating conditions of the ICP-MS were as follows: nebulizer gas flow of 0.91 L min^{-1}, ICP RF power of 950 W, lens voltage of 7 V, pulse stage voltage of 950 V and sample uptake rate of 26 rpm.

2.7. X-ray crystal structure determination

Important crystallographic data for the studied samples are listed in Table 1 (and Tables S1–S7 at supporting information). A black crystal of **1** (0.04, 0.06, 0.49 mm) was glued on a fiber and the data were collected at Room temperature. A yellow crystal of **2** (0.02, 0.11, 0.25 mm) and a colourless one of **3** (0.20, 0.23, 0.24 mm) were taken from the mother liquor and immediately cooled to −103 °C and to −113 °C, respectively. Diffraction measurements were made on a Rigaku R-AXIS SPIDER Image Plate diffractometer using graphite monochromated Mo Kα radiation. Data collection (ω-scans) and processing (cell refinement, data reduction and Empirical absorption correction) were performed using the CrystalClear program package [35]. The structures were solved by direct methods using SHELXS ver. 2013/1 [36] and refined by full-matrix least-squares techniques on F^2 with SHELXL ver.2014/6 [37]. Further experimental crystallographic details for **1**: $2\theta_{max}$ = 54.0°; reflections collected/unique/used, 13988/2955 [R_{int} = 0.0671]/2955; 93 parameters refined; $(\Delta/\sigma)_{max}$ = 0.002; $(\Delta\rho)_{max}/(\Delta\rho)_{min}$ = 1.175/−1.332 e/Å^3; *R*1/w*R*2 (for all data), 0.0515/0.0691. Further experimental crystallographic details for **2**: $2\theta_{max}$ = 54.0°; reflections collected/unique/used, 21109/3963 [R_{int} = 0.0674]/3963 parameters refined 147; $(\Delta/\sigma)_{max}$ = 0.002; $(\Delta\rho)_{max}/(\Delta\rho)_{min}$ = 1.286/−1.271 e/Å^3; *R*1/w*R*2 (for all data), 0.0194/0.0359. Further experimental crystallographic details for

Table 1
Crystallographic parameters for the prepared compounds.

Compound	(**1**)	(**2**)	(**3**)
Formula	$C_2H_7BiI_4N_2S_1$	$C_4H_{14}BiBr_5N_4S_2$	$C_4H_{14}BiCr_5N_4S_2$
Space group	P 2_1/a	$P2_12_12_1$	P 2_1/n
Z	4	4	8
a (Å)	7.8025(6)	8.5509 (5)	11.7775(3)
b (Å)	14.1381(9)	12.2296(7)	17.3827(4)
c (Å)	12.4458(9)	17.4594(10)	16.2788(4)
β	93.992(3)°	90.00°	91.2120(10)°
V (Å^3)	1369.6(2)	1825.8 (2)	3331.9(1)

3: $2\theta_{max}$ = 54.0°; reflections collected/unique/used, 30652/3619 [R_{int} = 0.0249]/3619 parameters refined 241; $(\Delta/\sigma)_{max}$ = 0.065; $(\Delta\rho)_{max}/(\Delta\rho)_{min}$ = 0.849/-0.352 e/Å^3; *R*1/w*R*2 (for all data), 0.0266/0.0492. Flack parameter x = -0.019(5) (Parson method [38]). Further experimental crystallographic details for **3** : the structure was solved and refined from a crystal presenting pseudomerohedral twinning i.e. the twin law (1,0,0/0,-1,0/-0.06,0,-1) is a 2-fold axis parallel to the [100] crystallographic direction and the refinement was performed with merged hkl5 (Rmerge = 0.052,total of 50,789 observations merged to 7622) data file and the BASF parameter was refined to the value 0.172(2), $2\theta_{max}$ = 54.0°; reflections used 7217; parameters refined 293; $(\Delta/\sigma)_{max}$ = 0.001; $(\Delta\rho)_{max}/(\Delta\rho)_{min}$ = 2.515/-1.810e/Å^3; *R*1/w*R*2 (for all data), 0.0458/0.1180. All hydrogen atoms in **1**, **2** and **3** were introduced at calculated positions as riding on bonded atoms. All non-hydrogen atoms for all structure were refined anisotropically. Plots of the structure were drawn using the Diamond 3 program package [39].

2.8. Optical studies

The absorption spectra were recorded with a Perkin–Elmer UV/Vis/NIR Lambda 19 spectrometer. The measurements were performed on thin films of the samples, prepared by rubbing crystals on a quartz surface. The photoluminescence spectrum of compound **1** was measured on a crystal under excitation with the 488 nm laser of the Renishaw inVia Raman microscope. The photoluminescence spectra of compounds **2** and **3** were recorded as films on quartz with the Jobin Yvon, Fluorolog 3 with excitation 350 nm and slits 5 nm for the excitation and 2 nm for the emission.

2.9. Vibronic studies

The Raman spectra were recorded with a Bruker RFS 100 FT-Raman spectrometer equipped with a neodymium-doped yttrium aluminium garnet laser [Nd-YAG, near-IR (NIR) line at λ = 1064 nm]. The power of the excitation radiation was 150 mW. FTIR-ATR spectra (500–4000 cm^{-1}) were measured on an Equinox 55 (Bruker Optics) spectrometer, equipped with a single-reflection diamond ATR accessory DuraSamplIR II (SensIR Technologies). Each spectrum represents an average of 128 scans at a resolution of 4 cm^{-1}.

2.10. Thermogravimetric analysis (TGA)

Thermogravimetric analysis (TGA) was performed using a TGA Q500 V20.2 Build 27 instrument by TA in an inert atmosphere of nitrogen. In a typical measurement, an amount of the material (~10 mg) was placed in the sample platinum pan, and the temperature was equilibrated at 40 °C. Subsequently, the temperature was increased to 700 °C with a rate of 5 °C/min, and the weight changes were recorded as a function of temperature.

2.11. Theoretical calculations

We used the WIEN2K computer package to perform our calculations [40]. The Kohn-Sham equations were solved using all-electron Full-Potential Linearized Augmented Plane Wave (FP-LAPW) method [41,42]. The exchange and correlation effects were treated by the Becke-Johnson functional [43]. In order to achieve a satisfactory degree of convergence of energy eigenvalues, the wave functions in the interstitial regions were expanded in plane wave up to R_{MT}*K_{max} equal to 4 (where $R_{MT}R_{MT}$ is the minimum radius of the muffin-tin-spheres and K_{max} gives the magnitude of the largest k vector in the plane wave expansion). Inside the atomic muffin-tin-spheres, the valence wave functions were expanded up to L_{max} = 10. The dependence of the total energy on the number of k-points in the irreducible wedge of the first Brillouin zone (BZ) has been explored within the linearized tetrahedron scheme [44]. The integrals over the BZ were performed up to 300 k-points and the size of the mesh has been set to 10*10*3 points. Self-consistency was achieved since the total energy difference between successive iterations was less than 10–5 Ryd per formula unit.

3. Results and discussion

3.1. Crystal structures

The compounds studied herein were obtained in a pure single crystal form. The crystals were large enough for X-ray crystal structure determination and investigation of their physical properties. Powder X-ray analysis for all compounds are similar with the theoretical calculated from the monocrystal data (Figs. S1–S3). In all three compounds the distances between the C and the two N atoms of the $CH_3SC(NH_2)_2^+$ cations are equal showing a resonance structure.

3.1.1. Crystal structure of compound 1

Compound **1** crystallizes in the monoclinic $P2_1/a$ space group. The anionic part of the structure consists of BiI_6^{-3} octahedral forming zig-zag chains along the a-axis through edge sharing (Fig. 1). The Bi–I bond lengths are around 2.92 Å for the non-bridging Bi-I bonds (Bi1-I2 and Bi1-I4) and from 3.0474(7) to 3.2971(6)Å, for the bridging Bi-I bonds (Table S2). The angles for I-Bi-I vary from 84.72(2)° to 95.83(2)° for the *cis* I and from 171.45(2)° to 175.33 (2)° for the *trans* I (Table S2). The deviation of the BiI_6 octahedron geometric parameters indicates their distorted character, which is a common characteristic of iodobismuthates either with inorganic [28,45] or organic cations [46]. This distortion of BiI_6 octahedral probably originates mainly from the repulsion of bismuth atoms between the adjacent BiI_6 building blocks [33]. This repulsion causes a contraction for the bridging angles, I3′-Bi1-I2 and I2″-Bi1-I3 (85.00°, 87.49°) and a widened of the non-bridging I1-Bi1-I4, 90.64(2)° (Table S2, Fig. 1a) [47]. Cations are arranged among the anionic chains and interact with them through hydrogen bonds (Fig. 1b, Table S3) forming layers parallel to the (001) plane. The anionic chains further interact through I···I interlayer contacts, which take values of 3.825 Å that are shorter than the sum of their Van der Waals radius (3.96 Å). In addition, interchain interactions are developed among chains belonging to neighbouring layers thus extending the interactions to 3D (Fig. 1c). Although these interactions take values of 4.104 Å which are a little longer than their Van der Waals sum, they are similar with previous reported values for similar materials [48]. These I···I interactions extend the anionic network along both the b- and c-axes producing a potential route for electronic interactions between the inorganic chains. There are I···I pathways repeating regularly along the chain axis involving a bridging and a terminal iodine from each chain.

3.1.2. Crystal structure of compound *2*

Compound **2** crystallizes in the orthorombic space group $P2_12_12_1$, with a stoichiometric formula $[CH_3SC(NH_2)_2]_2BiBr_5$ and the asymmetric unit of the cell contains one $BiBr_5^{-2}$ unit and two symmetry independent $CH_3SC(NH_2)_2$ cations. The anionic part of the structure consists of $BiBr_6^{-3}$ units, which are distorted octahedral forming zig-zag chains of corner sharing octahedral along the a-axis (Fig. 2a). The distortion of the octahedrals, is due to the Bismuth 6 s lone electron pair [49]. This comes in agreement with the Bi–Br bond lengths in the distorted $BiBr_6$ octahedral, which vary from 2.694 to 2.878 Å for the non-bridging bonds and take the values 2.959 and 3.058 Å, for the bridging ones

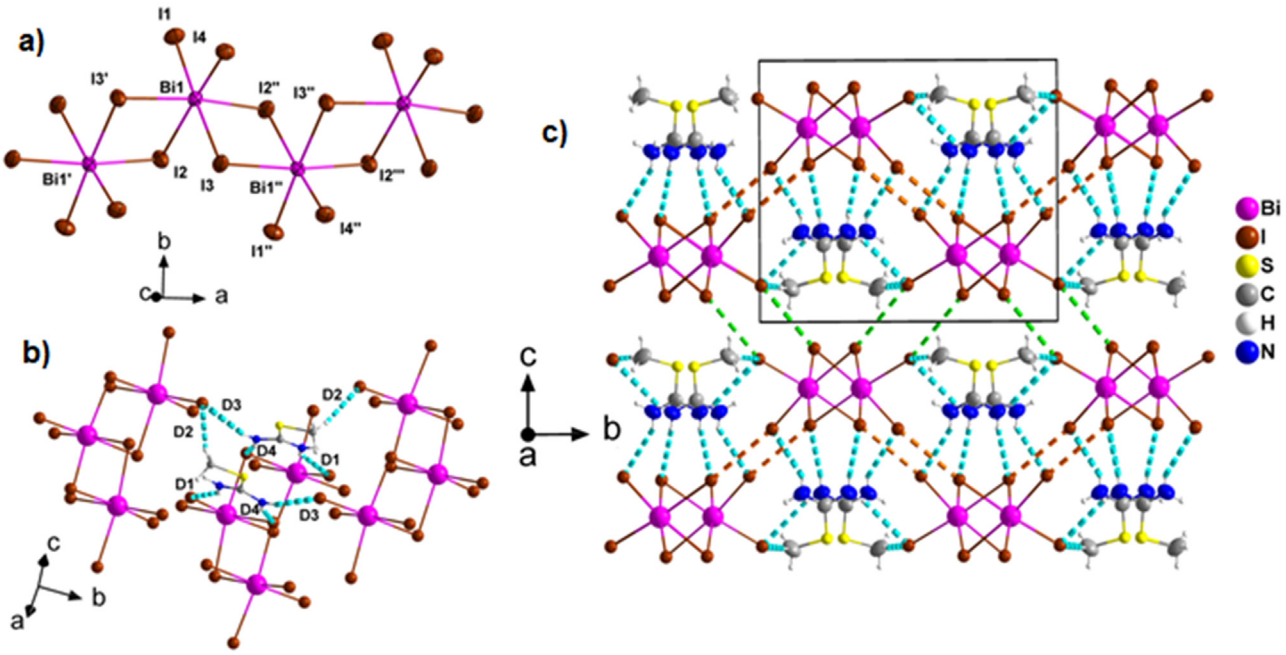

Fig. 1. a) Zigzag chains of BiI6-3 octahedral are formed parallel to the a-axis of compound 1. b) Hydrogen bond I···H interactions are formed among the zigzag anionic chains and the $CH_3SC(NH_2)_2^+$ cations and they are indicated with dashed cyan lines. The D1, D2, D3 and D4 symbols correspond to hydrogen bonds listed in Table S3. c) The zigzag chains through the hydrogen bonds interaction with the $CH_3SC(NH_2)_2^+$ cations forming layers parallel to the (001) plane. Intralayer and interlayer I···I contacts are indicated with brown and light green dashed lines respectively. Symmetry code: (′): −0.5 + *x*, 1.5 − *y*, *z*; (″): 0.5 + *x*, 1.5 − *y*, *z*; (‴): 1 + *x*, *y*, *z*.

(Table S4) The Br-Bi-Br angles vary from 86.54° to 94.10° for the *cis* Br and from 173.46° to 178.34° for the *trans* Br (Table S4). The two symmetry independent cations are arranged among the anionic chains and interact with them through hydrogen bonds and thus, build the 3D architecture of the structure (Fig. 2b, Table S5). Fig. 2c presents the 3D arrangement of anionic chains and cations and from this figure, it is clear that neighbouring anionic chains form a tweed structure and the angle between the planes defined by Bi atoms in each chain is equal to 58.97°.

3.1.3. Crystal structure of compound 3

Compound **3** is crystallized in the monoclinic P $2_1/n$ space group, with a stoichiometric formula $[CH_3SC(NH_2)_2]_2BiCl_5$ which is more accurately described by the formula $[CH_3SC(NH_2)_2]_4(BiCl_5)_2$ as there are two $BiCl_5^{-2}$ and four $CH_3SC(NH_2)_2^{+1}$ symmetry independent units in the asymmetric unit of the unit cell. The structure has been solved and refined from a twin crystal. At least, concerning the arrangement of the anionic chains structures **3** and **2** are similar. The structure consists of $BiCl_6^{-1}$ octahedra forming zig-zag chains parallel to the c-axis (Fig. 3a). The Bi–Cl bond lengths in the distorted $BiCl_6$ octahedra vary from 2.551 to 2.749 Å for the non-bridging bonds and from 2.818 to 2.909 Å, for the bridging ones (Table S6). The Cl-Bi-Cl angles vary from 84.93° to 93.53° for the cis Cl and from 176.31° to 178.86° for the *trans* Cl (Table S6). The four symmetry independent cations are arranged among the anionic chains and interact with them through hydrogen bonds thus contributing in the formation of the 3D architecture of the structure (Fig. 3b, Table S7). Fig. 3c presents the tweed arrangement of chains as in the structure of compound **2**. The angle between the planes defined by Bi atoms in each chain is equal to 77.88°.

3.2. Optical studies

Fig. 4a shows the UV – visible absorption and photoluminescence spectra of thin films of compound **1** prepared by rubbing crystals on the side of a quartz cell and measured at room temperature. At the absorption spectrum of compound **1**, three absorption bands are clearly observed at 2.26, 2.70 and 3.12 eV. The 1st band has the characteristic shape of excitonic absorption and according to several studies performed on similar low dimensional halobismuthates, it is assigned to the lowest excitons of the inorganic network [50]. This excitonic band is almost at the same energy as other 1D iodobismuthates [51,52], and significantly lower than 0D iodobismuthates [50,53,54]. In the bismuth (III) iodide based hybrids, the lowest exciton state is due to excitations from the valence band (consisting of Bi(6 s) state with some contribution from the iodide ligands Bi–I σ^*) to the conduction band (consisting, primarily of Bi(6p) states) [55].

The 2nd band is assigned to the electronic transition from the highest occupied molecular orbital (HOMO) to the lowest unoccupied molecular orbital (LUMO). These values are higher than those of 2D BiI_3 [56], similar with other 1D iodobismuthates [51–57] and smaller than the values of $(CH_3NH_3)_3Bi_2I_9$ [58] and other 0D analogues. The exciton binding energies are estimated to more than 440 meV.

Compound **1** shows also a very weak photoluminescence at 2.16 eV under excitation with a 488 nm laser. Although it is rare for the 1D iodobismuthates to have photoluminescence spectra there are some examples in the literature [22]. This photoluminescence probably is due to their pseudo two or three-dimensional character.

Compound **2** shows absorption bands at 2.94, 3.84, and 4.29 eV (Fig. 4b). The lowest energy band is assigned to the lowest excitons in the inorganic chain. The photoluminescence spectrum shows a narrow band at 2.64 eV that is assigned to the radiative recombination of the excitons located at the 1D inorganic part. The Stokes shift between the absorption and emission bands is relatively large (0.3 eV) and characterizes the strongly bounded excitons of the inorganic part that is common at the hybride perovskites. These values are similar with those of a the $(C_6H_{14}N)_2BiBr_5$ compound [59].

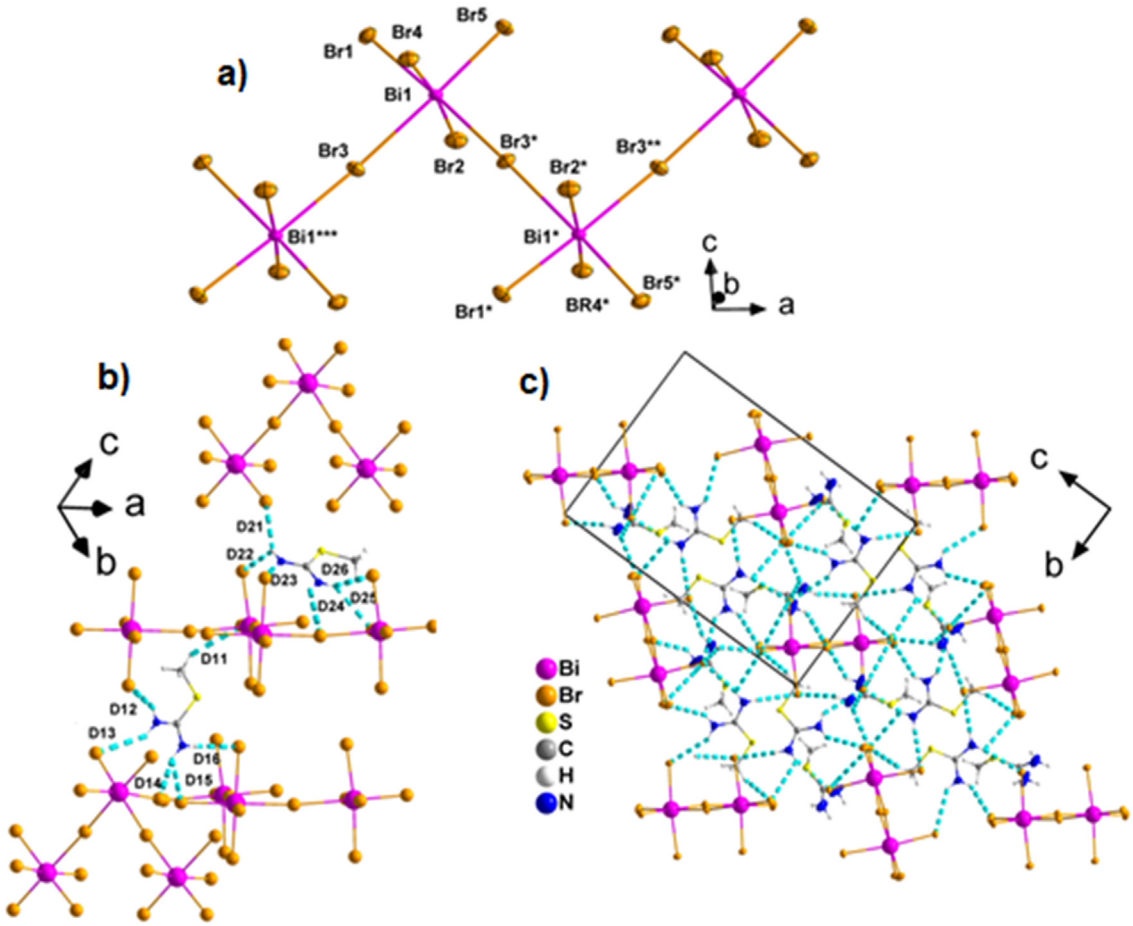

Fig. 2. a) Anionic chains parallel to the a-axis of compound 2. b) Hydrogen bond interactions of cations with the anionic chains. The dashed cyan lines indicate Br···H hydrogen bonds. The D11, D12, D13, D14, D21, D22, D23 and D24 symbols correspond to hydrogen bonds listed in Table S5. c) 3D arrangement of anionic chains and cations. Symmetry code: (*) 0.5 + *x*, 1.5 − *y*, −*z*; (**) 1 + *x*, *y*, *z*; (***) −0.5 + *x*, 1.5 − *y*, −*z*.

The absorption spectrum of compound **3** shows also an excitonic peak at 3.20 eV and peaks at 4.36 and 5.10 eV (Fig. 4c). These results are similar with the results obtained from chlorobismuthates with similar structure [51,60] and lower than that with a 0D structure [61].

In order to determine the optical band gaps, we calculated the Tauc plots based on the optical absorption spectra of compounds **1, 2** and **3** (Fig. 5). According to the DFT studies presented later on and compared to similar compounds, [27,33,62,63], all of the synthesized compounds **1**, **2**, **3** present a direct band gap at 2.30 3.32 and 3.67 eV, respectively. These suggestions are consistent with the dark red, yellow and white color of the compound **1**, **2**, **3** crystals respectively.

3.3. Vibronic studies

The IR spectrum in the area 500–3500 cm^{-1} (Fig. S4) is due to the organic part and is similar for the three salts. The peaks at 3000 and 2926 cm^{-1} are due to the CH stretch. The peaks at 1625, 1533 and 1426 cm^{-1} are assigned to the $\delta_{as}(NH_2)$, $\delta_s(NH_2)$ and to the $\nu_{as}(CN)$ vibrations respectively. The peaks above 3000 cm^{-1} are assigned to N—H stretch [64]. The spectra are similar with those of other salts with the same amine.

The organic–inorganic interaction is strongly dictated by hydrogen bonding between the NH_3^+ groups and the halide atoms. The positions of the IR and Raman bands associated to N—H are depended from the strength of the hydrogen bonding with the halide atoms. For that reason, vibrational spectroscopy is a powerful tool for the investigation of the interaction of the organic cation with the surrounding environment created from the Bi-Halogen perovskite subunits [65]. From I to Cl the hydrogen bonding increase and the corresponding N—H peaks appear to higher frequencies (Fig. 6). The characteristic vibrations due to the Bi-X bonds can be seen at the Raman spectrum at frequencies lower than 300 cm^{-1}: (Fig. 7).

Similarly, the part of Raman spectra at frequencies higher than 400 cm^{-1} is mainly due to the organic part and is almost similar for the three salts and similar to other salts of the amine (supporting information Fig. S5).

The $[CH_3SC(NH_2)_2]BiI_4$, **1**, has a symmetry of the type C_{2v}. It has two stretching vibrations for the external Iodides ($A_1 + B_1$), four for the bridging Iodides ($2A_1 + B_1 + B_2$) and 9 bending vibrations ($3A_1 + 2A_2 + 2B_1 + 2B_2$). From these, four are Raman active ($A_1 + A_2 + B_1 + B_2$).

The Raman spectrum of compound $[CH_3SC(NH_2)_2]BiI_4$ has two strong peaks at 135 cm^{-1} and 105 cm^{-1} that can be assigned at the Bi–I stretching for the external and bridging I respectively [57,66], and three weak peaks at 91, 78 and 64 cm^{-1} that can be assigned to bending modes.

The $[CH_3SC(NH_2)_2]_2BiX_5$ (X = Br, Cl) has a symmetry of the type C_{2v}. So, it has four stretching vibrations for the external halogens ($2A_1 + B_1 + B_2$), two for the bridging halogens ($A_1 + B_1$) and 9 bending vibrations ($3A_1 + 2A_2 + 2B_1 + 2B_2$). From these four are expected to be Raman active ($A_1 + A_2 + B_1 + B_2$).

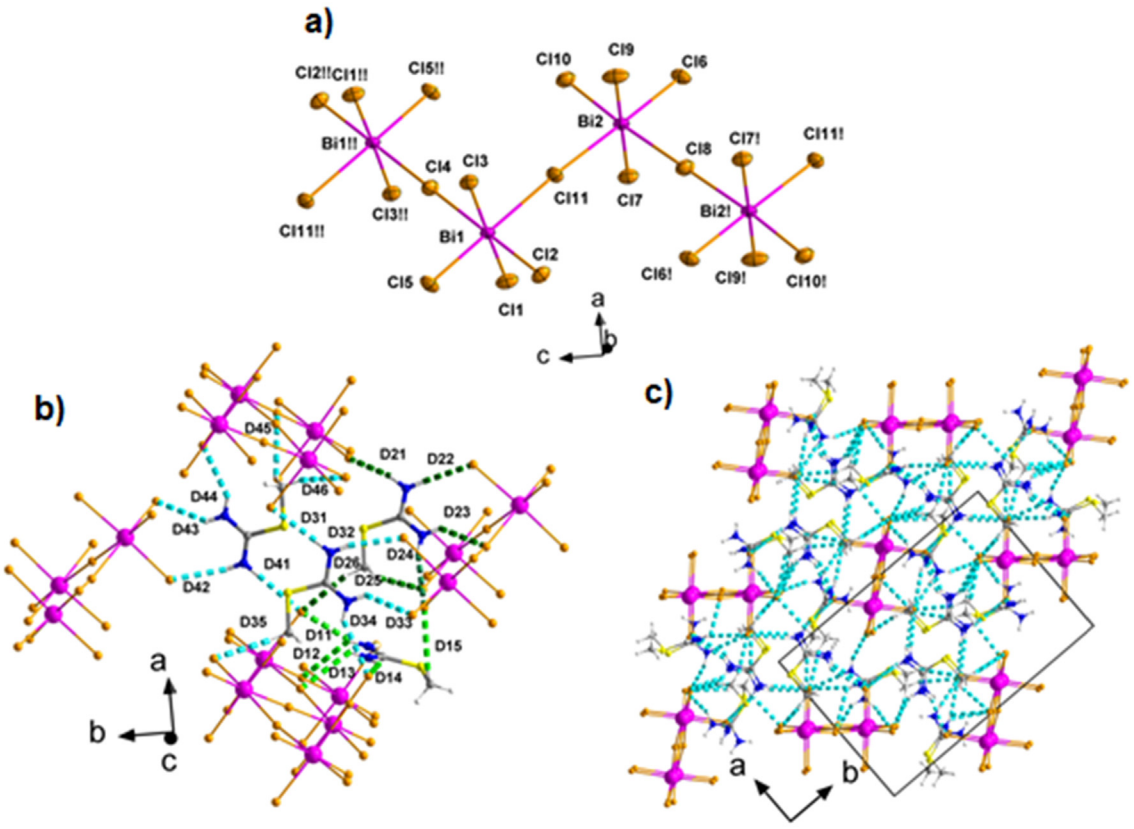

Fig. 3. a) Chains parallel to the c-axis of compound **3**. b) Hydrogen bond interactions of cations with the anionic chains. The dashed cyan lines indicate Cl···H hydrogen bonds. The D11, D12, D13, D14, D15, D21, D22, D23, D24, D25, D26, D31, D32, D33, D34, D35, D41, D42, D43, D44 and D45 symbols correspond to hydrogen bonds listed in Table S7. c) 3D arrangement of anionic chains and cations. Symmetry code: (!) 2 − *x*, 1 − *y*, 1 − *z*; (!!) 2 − *x*, 1 − *y*, 2 − *z*.

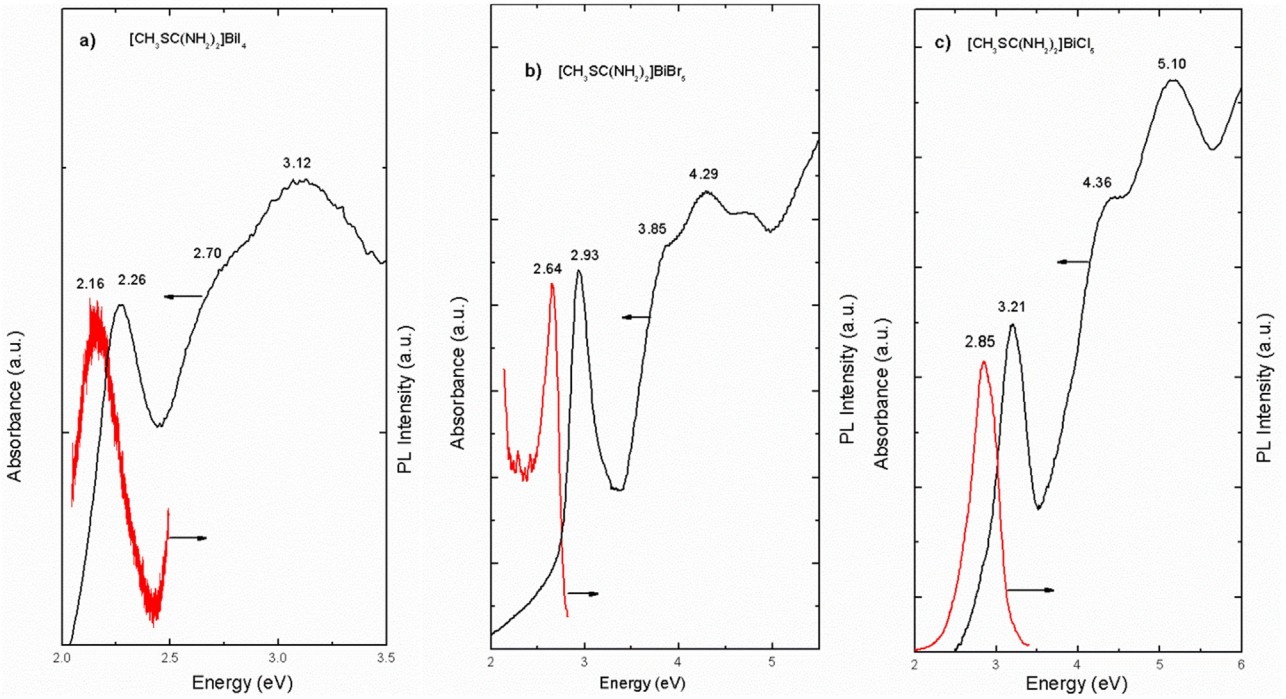

Fig. 4. Optical absorption and photoluminescence spectra, at room temperature of thin films of compound **1** a), **2** b) and **3** c).

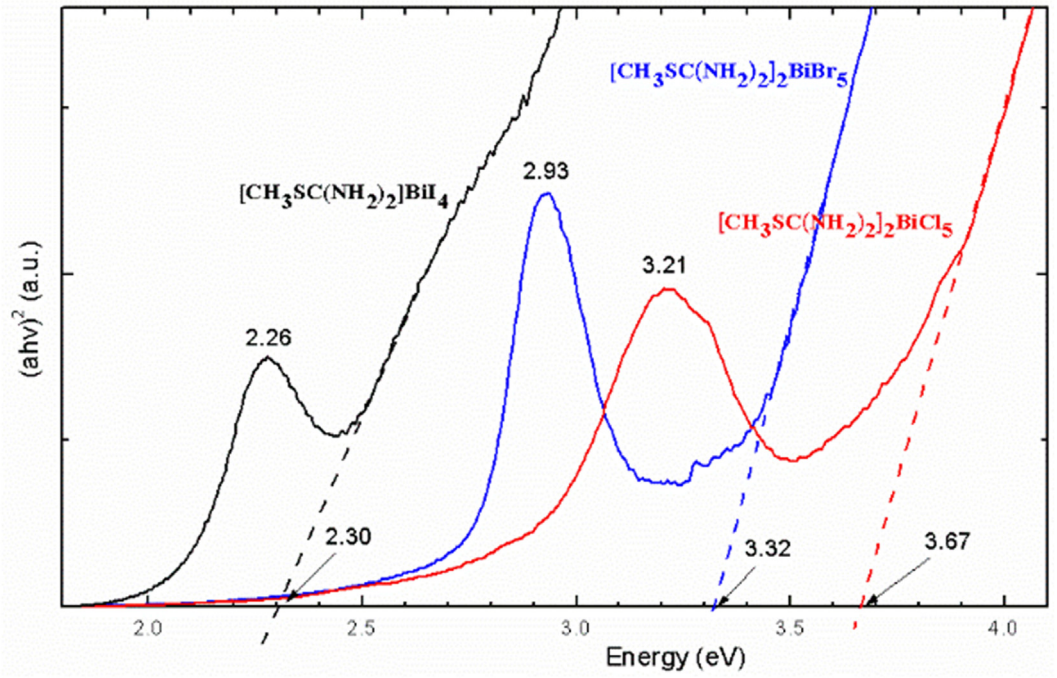

Fig. 5. Tauc-Plots of compounds **1**, **2** and **3**, calculated from the optical absorption spectra of thin films at room temperature.

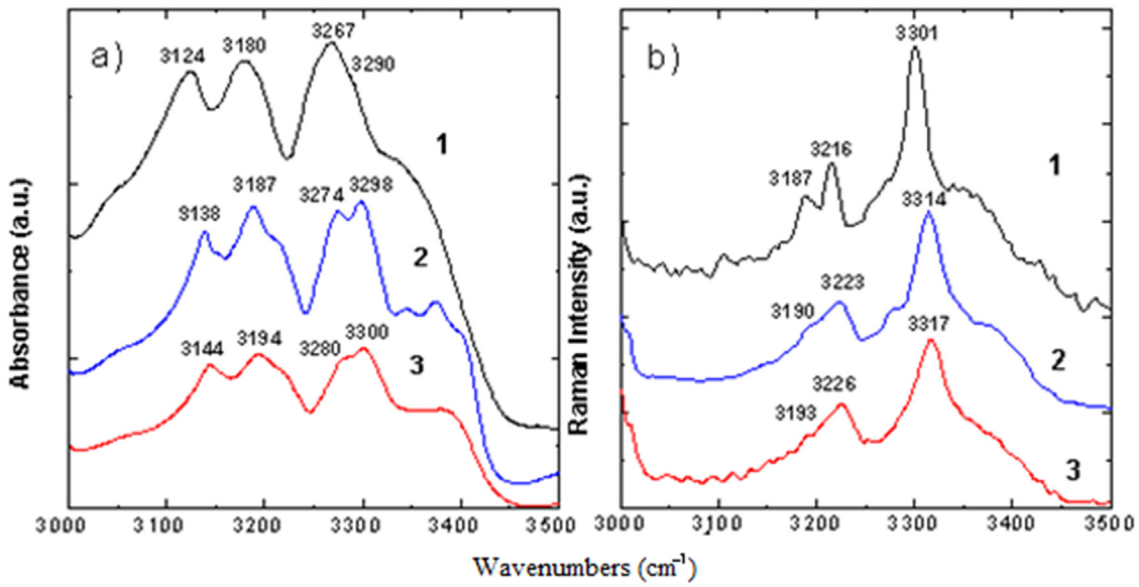

Fig. 6. a) IR and b) Raman spectra of salts **1**, **2** and **3**, in the region 3000–3500 cm^{-1}.

The Raman spectrum of compound **2**, has two strong peaks at 180 and 159 cm^{-1} that can be assigned at the Bi–Br stretching for the external (*cis* and *trans*) BiBr vibration [67], a smaller peak at 142 cm^{-1} assigned to the bridging Br [67], and a broad band around 100 cm^{-1} that can be assigned to bending modes [59].

The Raman spectrum of compound **3**, has a strong and broad peak at 258 cm^{-1} that can be assigned at the Bi–Cl stretching for the external BiCl vibration and another peak at 176 cm^{-1} assigned to the bridging Cl. The broad band at 100 cm^{-1} can be assigned at the bending modes [60].

3.4. Thermogravimetric analysis

Thermogravimetric analysis results for the compounds and one of the starting amines are presented in Fig. S6. The experiments were performed on a 40% N_2 – 60% O_2 atmosphere. In almost all the cases decomposition starts ≈190 °C. There are three main decomposing procedures that are present also in the amine. At 500 °C the total mass loss is almost 100% for the compounds **1** and **2** and 37% for the compound **3**. The loss of the inorganic part is probably due to sublimation of the salts.

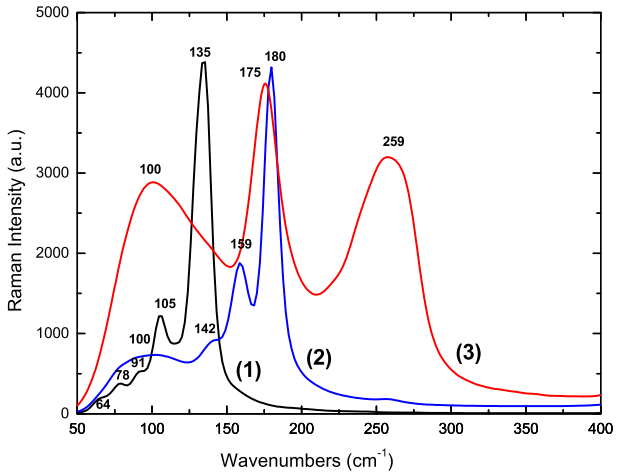

Fig. 7. Raman spectra of compounds **1**, **2** and **3**, in the region 50–400 cm^{-1}.

3.5. DFT studies

Periodic DFT calculations were performed on the three compounds. The calculated direct band gaps are 2.6, 2.9 and 3.6 eV for compounds **1, 2** and **3** respectively.

The calculated band gaps for compounds **1** and **3** slightly overestimate the estimated gaps by the Tauc plots.

The electronic band structures show that the three compounds have a direct band gap at the Γ point of the Brillouin zone (Fig. 8) as in the case of similar compounds [33,45].

The dispersion curves are flat for most of the directions in the first Brillouin zone, which is characteristic of the low dimensionality for these compounds.

The partial density of states (P-DOS) show that the edge of the valence band is mainly composed by Bi *6p*/I *5p* states for **1** (Fig. 9a), Bi *6p*/Br *4p* states for compound **2** (Fig. 9b) and Bi *6p*/Cl *3p* states for compound **3** (Fig. 9c). On the other hand, the conduction band is mainly made up of Bi 6p states for the three compounds. The small overlap between the Bi-*6s* and the X-*p* (X = I, Br, Cl) wavefunctions (and thus the weak Bi-X hybridization) is due to the distortion of the BiX_6 octahedra. At high energy, both CB and VB, have weak contributions from the organic cations electronic states.

Based on these results, we can deduce that the main optical properties for the three compounds, near their band gaps, originate mainly from the inorganic chains.

4. Conclusions

Three new organic–inorganic materials based on bismuth were synthesized and characterized. All of them have a 1D inorganic

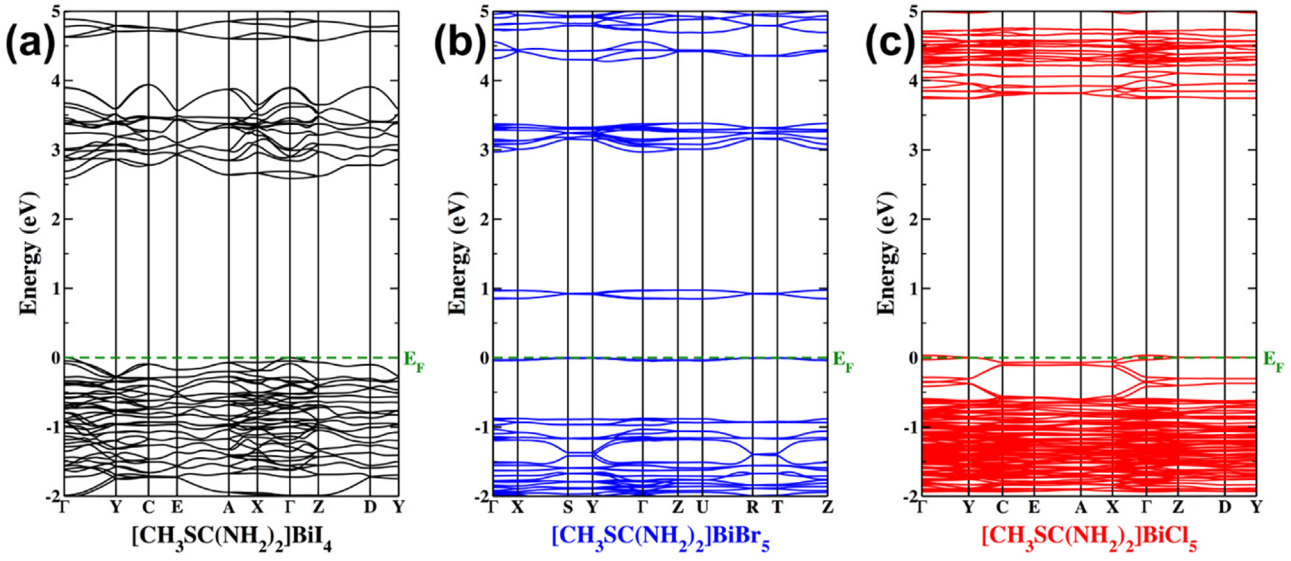

Fig. 8. Calculated band structures for (a) compound **1**, (b) compound **2** and (c) compound **3**.

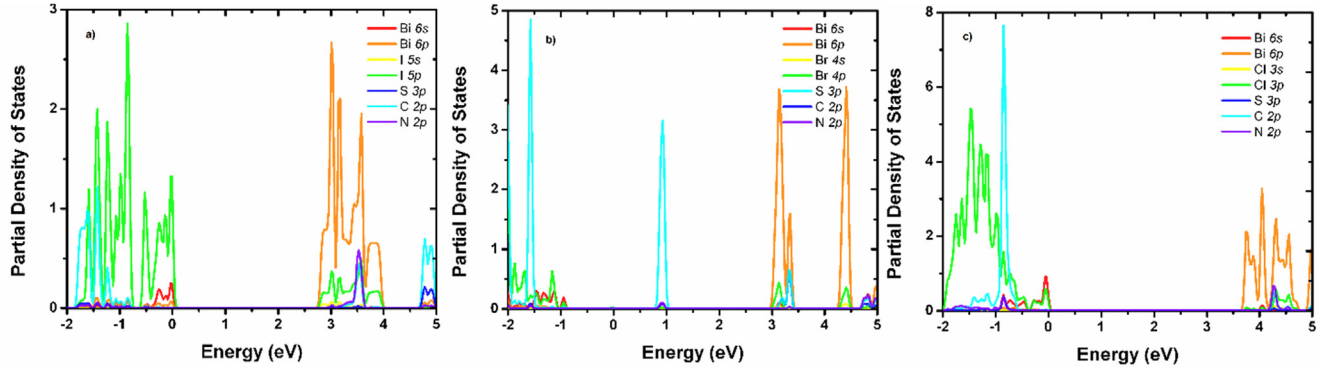

Fig. 9. P-DOS of compounds **1(a)**, **2(b)**, **3(c)**.

structure that consists of edge (compound **1**) or corner (compounds **2**, **3**) sharing octahedral forming zigzag columns separated by the organic moieties. In the case of the compound **1,** there are short I···I distances between the different columns forming a pseudo 3D network. All of them show strong absorption at the UV region and the compounds **1** and **2** show weak luminescence. In addition, they are stable up to 150° C that is higher than the usual heat-treating temperature for this kind of materials. Concerning their physical properties, although they have higher E_g than the corresponding lead based 3D perovskites, they are non-toxic and they are more stable. Similar materials have been tested as candidates to replace lead-based dyes at photovoltaic devices but they have small efficiencies. Band structure calculations show a pretty good agreement with the experimental data. Appropriate molecular design can improve the properties and solar cell performance of bismuth based perovskite materials filling the gap with the state-of-the-art Pb-based perovskite devices [68]. These new materials may find applications also in other perovskite devices such as light-emitting diodes and photodetectors.

Acknowledgements

This work is supported by the ERANET-MED-ENERG-11-132 project: "HYDROSOL". by the "Greek General Secretariat of Research and Technology" (MIS T3EPA-00029) which is implemented under the "European R & D Collaboration – Granting Operation of Greek Bodies Successfully in Common Notice For Proposals Of The European Networks Era-Net" funded by the Operational Programme "Competitiveness, Entrepreneurship and Innovation" (NSRF 2014-2020) and co-financed by Greece and the European Union (European Regional Development Fund), and by the Ministry of High Education of Tunisia.

Appendix A. Supplementary data

CCDC 1898437, 1898438 and 1898439 contains the supplementary crystallographic data for compound 1, compound 2 and compound 3, respectively. These data can be obtained free of charge via http://www.ccdc.cam.ac.uk/conts/retrieving.html, or from the Cambridge Crystallographic Data Centre, 12 Union Road, Cambridge CB2 1EZ, UK; fax: (+44) 1223-336-033; or e-mail: deposit@ccdc.cam.ac.uk.

Supplementary data to this article can be found online at https://doi.org/10.1016/j.poly.2019.114180.

References

[1] C.C. Stoumpos, C.D. Malliakas, M.G. Kanatzidis, Inorg. Chem. 52 (2013) 9019, https://doi.org/10.1021/ic401215x.
[2] G. Xing, N. Mathews, S. Sun, S.S. Lim, Y.M. Lam, M. Grätzel, S. Mhaisalkar, T.C. Sum, Science 342 (2013) 344, https://doi.org/10.1126/science.1243167.
[3] S.D. Stranks, G.E. Eperon, G. Grancini, C. Menelaou, M.J.P. Alcocer, T. Leijtens, M. L. Herz, A. Petrozza, H.J. Snaith, Science 342 (2013) 341, https://doi.org/10.1126/science.1243982.
[4] G.C. Papavassiliou, G.A. Mousdis, I.B. Koutselas, Adv. Mater. Opt. Electron. 9 (1999) 265, https://doi.org/10.1002/1099-0712(199911/12)9:63.3.CO;2-Y.
[5] G.C. Papavassiliou, G.A. Mousdis, I. Koutselas, Monatsh. Chem. 132 (2001) 113, https://doi.org/10.1007/s007060170150.
[6] W. Bi, N. Louvain, N. Mercier, J. Luc, I. Rau, F. Kajza, B. Sahraoui, Adv. Mater. 20 (2008) 1013, https://doi.org/10.1002/adma.200701753.
[7] G.C. Papavassiliou, G.A. Mousdis, G. Pagona, N. Karousis, M.-S. Vidali, J. Lumin. 149 (2014) 287, https://doi.org/10.1016/j.jlumin.2014.01.050.
[8] H. Abid, A. Samet, A. Mlayah, H. Boughzala, Y. Abid, Opt. Mat. 73 (2017) 89, https://doi.org/10.1016/j.optmat.2017.07.050.
[9] G.A. Mousdis, G.C. Papavassiliou, C.P. Raptopoulou, A. Terzis, J. Mater. Chem. 10 (2000) 515, https://doi.org/10.1039/A906161D.
[10] A. Mousdis, V. Gionis, G.C. Papavassiliou, C.P. Raptopoulou, A. Terzis, J. Mater. Chem. 8 (1998) 2259, https://doi.org/10.1039/A802926A.
[11] A. Samet, A.B. Ahmed, A. Mlayah, H. Boughzala, E.K. Hlil, Y. Abid, J. Mol. Struct. 977 (2010) 72, https://doi.org/10.1016/j.molstruc.2010.05.016.
[12] M.M. Lee, J. Teuscher, T. Miyasaka, T.N. Murakami, H.J. Snaith, Science 338 (2012) 643, https://doi.org/10.1126/science.1228604.
[13] J. Qi, C. Zema, W. Pengyang, Y. Xiaolei, L. Heng, W. Ye, Y. Zhigang, W. Jinliang, Z. Xingwang, Y. Jingbi, Adv. Mater. 29 (2017) 1703852, https://doi.org/10.1002/adma.201703852.
[14] S. Ryu, J. Seo, S.S. Shin, Y.C. Kim, N.J. Jeon, J.H. Noh, S.I. Seok, J. Mat. Chem. A 13 (2015) 3271, https://doi.org/10.1039/C5TA00011D.
[15] A. Kojima, K. Teshima, Y. Shirai, T. Miyasaka, J. Am. Chem. Soc. 131 (2009) 6050, https://doi.org/10.1021/ja809598r.
[16] National Renewable Energy Laboratory, best research-cell efficiencies chart https://www.nrel.gov/pv/assets/images/efficiency-chart.png.
[17] W.S. Yang, B.-W. Park, E.H. Jung, N.J. Jeon, Y.C. Kim, D.U. Lee, S.S. Shin, J. Seo, E. K. Kim, J.H. Noh, S. Seok, Science 356 (2017) 1376, https://doi.org/10.1126/science.aan2301.
[18] G.C. Papavassiliou, G.A. Mousdis, A. Terzis, C.P. Raptopoulou, Z. Naturforsch. 58b (2003) 815, https://doi.org/10.1515/znb-2003-0817.
[19] A. Samet, H. Boughzala, H. Khemakhem, Y. Abid, J. Mol. Struct. 984 (2010) 23, https://doi.org/10.1016/j.molstruc.2010.08.049.
[20] A. Vassilakopoulou, D. Papadatos, I. Zakouras, I. Koutselas, J. Alloys Comp. 692 (2017) 589, https://doi.org/10.1016/j.jallcom.2016.09.076.
[21] A. Yangui, S. Pillet, E. Bendeif, A. Lusson, S. Triki, Y. Abid, K. Boukheddaden, ACS Photonics 5 (2018) 1599, https://doi.org/10.1021/acsphotonics.8b00052.
[22] W. Zhang, K. Tao, C. Ji, Z. Sun, S. Han, J. Zhang, Z. Wu, J. Luo, Inorg. Chem. 57 (2018) 4239, https://doi.org/10.1021/acs.inorgchem.8b00152.
[23] G. Lanty, A. Bréhier, R. Parashkov, J.S. Lauret, E. Deleporte, New J. Phys. 10 (2008), https://doi.org/10.1088/1367-2630/10/6/065007 065007.
[24] C.R. Kagan, D.B. Mitzi, C.D. Dimitrakopoulos, Science 286 (1999) 945, https://doi.org/10.1126/science.286.5441.945.
[25] A.M. Ganose, C.N. Savory, D.O. Scanlon, Chem. Commun. 53 (2017) 20, https://doi.org/10.1039/C6CC06475B.
[26] R.E. Brandt, R.C. Kurchin, R.L.Z. Hoye, J.R. Poindexter, M.W.B. Wilson, S. Sulekar, F. Lenahan, P.X.T. Yen, V. Stevanović, J.C. Nino, M.G. Bawendi, T. BuonassisiJ, Phys. Chem. Lett. 6 (2015) 4297, https://doi.org/10.1021/acs.jpclett.5b02022.
[27] B.-W. Park, B. Philippe, X. Zhang, H. Rensmo, G. Boschloo, E.M.J. Johansson, Adv. Mat. 27 (2015) 6806, https://doi.org/10.1002/adma.201501978.
[28] A.N. Usoltsev, M. Elshobaki, S.A. Adonin, L.A. Frolova, T. Derzhavskaya, P.A. Abramov, D.V. Anokhin, I.V. Korolkov, S.Y. Luchkin, N.N. Dremova, K.J. Stevenson, M.N. Sokolov, V.P. Fedin, P.A. Troshin, J. Mat. Chem. A 7 (2019) 5957, https://doi.org/10.1039/C8TA09204D.
[29] D.M. Fabian, S. Ardo, J. Mat. Chem. A 4 (2016) 6837, https://doi.org/10.1039/C6TA00517A.
[30] H. Wang, J. Tian, K. Jiang, Y. Zhang, H. Fan, J. Huang, L.-M. Yang, B. Guan, Y. Song, RSC Adv. 7 (2017) 43826, https://doi.org/10.1039/C7RA07123J.
[31] A. Kulkarni, T. Singh, M. Ikegami, T. Miyasaka, RSC Adv. 7 (2017) 9456, https://doi.org/10.1039/C6RA28190G.
[32] M.E. Kamminga, A. Stroppa, S. Picozzi, M. Chislov, I.A. Zvereva, J. Baas, A. Meetsma, G.R. Blake, T.T.M. Palstra, Inorg. Chem. 56 (2017) 33, https://doi.org/10.1021/acs.inorgchem.6b01699.
[33] T. Li, Y. Hu, C.A. Morrison, W. Wu, H. Han, N. Robertson, Sustain. Energ. Fuels 1 (2017) 308, https://doi.org/10.1039/C6SE00061D.
[34] G.A. Mousdis, N.-M. Ganotopoulos, H. Barkaoui, Y. Abid, V. Psycharis, A. Savvidou, C.P. Raptopoulou, Eur. J. Inorg. Chem. 2017 (2017) 3401, https://doi.org/10.1002/ejic.201700277.
[35] M.S.C. Rigaku, CrystalClear, Rigaku/MSC Inc., The Woodlands, Texas, USA, 2005.
[36] G.M. Sheldrick, Acta Cryst. A 64 (2008) 112, https://doi.org/10.1107/S0108767307043930.
[37] G.M. Sheldrick, Acta Cryst. C 71 (2015) 3, https://doi.org/10.1107/S2053229614024218.
[38] S. Parson, H.D. Flack, T. Wagner, Acta Cryst. B 69 (2013) 249, https://doi.org/10.1107/S2052519213010014.
[39] DIAMOND – Crystal and Molecular Structure Visualization, Ver. 3.1, Crystal Impact, Rathausgasse 30, 53111, Bonn, Germany.
[40] P. Blaha, K. Schwarz, G.K.H. Madsen, D. Kvasnicka, J. Luitz, R. Laskowski, F. Tran, L. D., Marks WIEN2k An Augmented Plane Wave plus Local Orbitals Program for Calculating Crystal Properties, Vienna University of Technology, Austria, 2001.
[41] G.K.H. Madsen, P. Blaha, K. Schwarz, E. Sjöstedt, L. Nordström, Phys. Rev. B 64 (2001), https://doi.org/10.1103/PhysRevB.64.195134 195134.
[42] K. Schwarz, P. Blaha, G.K.H. Madsen, Comput. Phys. Commun. 147 (2002) 71, https://doi.org/10.1016/S0010-4655(02)00206-0.
[43] A.D. Becke, E.R. Johnson, J. Chem. Phys. 14 (2006), https://doi.org/10.1063/1.2213970 221101.
[44] P.E. Blöchl, O. Jepsen, O.K. Andersen, Phys. Rev. B 49 (1994) 16223, https://doi.org/10.1103/PhysRevB.49.16223.
[45] N.A. Yelovik, A.V. Mironov, M.A. Bykov, A.N. Kuznetsov, A.V. Grigorieva, Z. Wei, E.V. Dikarev, A.V. Shevelkov, Inorg. Chem. 55 (2016) 4132, https://doi.org/10.1021/acs.inorgchem.5b02729.
[46] P.A. Buikin, A.B. Ilyukhin, A.E. Baranchikov, K.E. Yorov, V.Y. Kotov, Mendeleev Commun. 28 (2018) 490, https://doi.org/10.1016/j.mencom.2018.09.012.
[47] K. Eckhardt, V. Bon, J. Getzschmann, J. Grothe, F.M. Wisser, S. Kaskel, Chem. Commun. 52 (2016) 3058, https://doi.org/10.1039/C5CC10455F.
[48] N. Louvain, N. Mercier, F. Boucher, Inorg. Chem. 48 (2009) 879, https://doi.org/10.1021/ic801900r.
[49] A. Buikin, A.Y. Rudenko, A.E. Baranchikov, A.B. Ilyukhin, V.Y. Kotov, Russ. J. Coord. Chem. 44 (2018) 373, https://doi.org/10.1134/S1070328418060015.

[50] H. Dammak, A. Yangui, S. Triki, Y. Abid, H. Feki, J. Lumin. 161 (2015) 214, https://doi.org/10.1016/j.jlumin.2015.01.010.
[51] G.A. Mousdis, G.C. Papavassiliou, A. Terzis, C.P. Raptopoulou, Z. Naturforsch. 53b (1998) 927, https://doi.org/10.1515/znb-1998-0825.
[52] C. Hrizi, N. Chaari, Y. Abid, N. Chniba-Boudjada, S. Chaabouni, Polyhedron 46 (2012) 41, https://doi.org/10.1016/j.poly.2012.07.062.
[53] T. Kawai, S. Shimanuki, Phys. Status Solidi B 177 (1993) K43, https://doi.org/10.1002/pssb.2221770128.
[54] V.Y. Kotov, A.B. Ilyukhin, A.A. Korlyukov, A.F. Smol'yakov, S.A. Kozyukhin, New J. Chem. 42 (2018) 6354, https://doi.org/10.1039/C7NJ04948J.
[55] M.A. Tershansy, A.M. Goforth, J.R. Gardinier, M.D. Smith, L. Peterson Jr., H.-C. Zur Loye, Solid State Sci. 9 (2007,) 410, https://doi.org/10.1016/j.solidstatesciences.2007.03.010.
[56] R.E. Brandt, R.C. Kurchin, R.L.Z. Hoye, J.R. Poindexter, M.W.B. Wilson, S. Sulekar, F. Lenahan, P.X.T. Yen, V. Stevanović, J.C. Nino, M.G. Bawendi, T. Buonassisi, J. Phys. Chem. Lett. 6 (2015) 4297, https://doi.org/10.1021/acs.jpclett.5b02022.
[57] C. Hrizi, A. Samet, Y. Abid, S. Chaabouni, M. Fliyou, A. Koumina, J. Mol. Struct. 992 (2011) 96, https://doi.org/10.1016/j.molstruc.2011.02.051.
[58] T. Kawai, A. Ishii, T. Kitamura, S. Shimanuki, M. Iwata, Y. Ishibashi, J. Phys. Soc. Jpn. 65 (1996) 1464, https://doi.org/10.1143/JPSJ.65.1464.
[59] H. Dammak, S. Triki, A. Mlayah, Y. Abid, H. Feki, J. Lumin. 166 (2015) 180, https://doi.org/10.1016/j.jlumin.2015.05.031.
[60] H. Ferjani, H. Boughzala, J. Mat. 2014 (2014), https://doi.org/10.1155/2014/253602 253602.
[61] D. Fredj, C.B. Hassen, S. Elleuch, H. Feki, N.C. Boudjada, T. Mhiri, M. Boujelbene, Mater. Res. Bull. 85 (2017) 23, https://doi.org/10.1021/acsami.7b16297.
[62] M. Pazoki, M.B. Johansson, H. Zhu, P. Broqvist, T. Edvinsson, G. Boschloo, E.M.J. Johansson, J. Phys. Chem. C 120 (2016) 29039, https://doi.org/10.1021/acs.jpcc.6b11745.
[63] C.C. Stoumpos, L. Frazer, D.J. Clark, Y.S. Kim, S.H. Rhim, A.J. Freeman, J.B. Ketterson, J.I. Jang, M.G. Kanatzidis, J. Am. Chem. Soc. 137 (2015) 6804, https://doi.org/10.1021/jacs.5b01025.
[64] R. Keuleers, H.O. Desseyn, B. Rousseau, C. Van Alsenoy, J. Phys. Chem. A 103 (1999) 4621, https://doi.org/10.1021/jp984180z.
[65] G.C. Anyfantis, N.-M. Ganotopoulos, A. Savvidou, C.P. Raptopoulou, V. Psycharis, G.A. Mousdis, Polyhedron 151 (2018) 299, https://doi.org/10.1016/j.poly.2018.05.024.
[66] G.Y. Ahlijah, M. Goldstein, J. Chem. Soc. A (1970) 326, https://doi.org/10.1039/J19700000326.
[67] J. Laane, P.W. Jagodzinski, Inorg. Chem. 19 (1980) 44, https://doi.org/10.1021/ic50203a010.
[68] V.Y. Kotov, A.B. Ilyukhin, K.P. Birin, V.K. Laurinavichyute, A.A. Sadovnikov, Z.V. Dobrokhotova, S.A. Kozyukhin, New J. Chem. 40 (2016) 10041, https://doi.org/10.1039/C6NJ02333A.